Proceedings World Geothermal Congress 2023
Beijing, China, April 17 – 21, 2023

Flexible Geothermal Power Dispatch Using Thermal Storage Tanks

Mohammad J. Aljubran and Roland N. Horne

Stanford Geothermal Program, Stanford, California 94305, United States

aljubrmj@stanford.edu

Keywords: Dispatch; Power; Thermal Storage

ABSTRACT

Dispatchable energy resources are key for reliable power supply. Whereas the development of fossil fuel resources has dominated the supply for dispatchable capacity, this trend is forecasted to slow down due to the growing climate change concerns and transition to renewable resources. Geothermal energy has always been an economical resource for district heating and baseload power. With the decline of fossil fuel plants, geothermal facilities have been expanding beyond baseload to supply flexible heat and electricity. There is only a limited number of studies that investigate approaches to facilitate flexible geothermal power generation, mainly focused on steam vent-off, wellhead throttling, turbine inlet pressure control, and turbine bypass. This study reviewed the common approaches of dispatchable geothermal power generation, and particularly evaluated the techno-economics of surface thermal storage tanks.

We examined a 200° C, liquid-dominated geothermal resource developed with 5 producers and 5 injectors alongside an 80-MWe subcritical Organic Rankine Cycle (ORC) power plant. We used a conceptual subsurface model to simulate temperature decline over time alongside correlations to estimate power plant efficiency under different operating conditions. Specifying financial parameters, we estimated a levelized cost of electricity ($LCOE$) of 43 $\$/MWh$. We then added a 17 $\$million$ surface storage tank with capacity of 11,830 m^3. Tank heat losses were modeled based on heat transfer principles of conduction, convection and radiation, alongside thermodynamic equilibria. With 2021 real-time electricity market prices retrieved from the California Independent System Operator database, we evaluated the scenario in which the tank is charged daily during the four hours with the lowest prices and discharged during the 16 hours of the highest prices. Flexible power generation results in a net present value (NPV) increase of 8.41 $\$million$ compared to the baseline scenario of baseload power generation during positively priced time intervals.

This work demonstrates the techno-economic potential of installing surface thermal storage tanks to achieve flexible geothermal power generation to fit into a grid with significant intermittency. It also showcases the role geothermal resources could play in grid decarbonization efforts where power reliability is a challenge.

1. INTRODUCTION

The California net-zero carbon economy has been dependent on the rapid growth of solar and wind electricity, as well as electrification of transportation and heating. However, the increasing reliance on weather-dependent renewables can raise grid reliability challenges which mandates careful resource planning. This raises the need for "clean firm power": carbon-free power resources that are always available for as long as needed. Diversity of resources across dispatch capabilities is also desirable and found to further reduce the costs of full grid decarbonization (Long et al. 2021). Generally, a renewable resource is more appealing when it can cost-effectively integrate in the energy mix and shift its power output to span diverse forms of dispatch, e.g., baseload, hourly, daily, and seasonal.

Geothermal energy provides clean firm power, where it is historically viewed as a baseload or "always-on" resource with high capacity factors. Given the high upfront risk and capital expenditure, geothermal power operators typically operate under power purchase agreements (PPAs). However, the high penetration of intermittent resources caused an increase in the value for dispatchable geothermal generation that would fill in the diurnal and seasonal gaps. Under the Grid Modernization Initiative launched by the U.S. Department of Energy (DOE), the Geothermal Technologies Office invested in the Beyond Batteries initiative which aims to integrate geothermal energy into flexible and controllable resource through underground storage (Dobson et al. 2020). In the 2021 U.S. Geothermal Power Production and District Heating Market Report, the National Renewable Energy Laboratory (NREL) identified dispatchable geothermal energy as one of the top ten emerging geothermal technologies (Robins et al. 2021). Hence, there is need for further techno-economic analysis to evaluate the economics and requirements of flexible geothermal operations for future decarbonized electricity grids. This paper reviews the different operational implementations used to enable dispatchable power generation, and particularly discusses the technical and economic viability of using surface thermal storage tanks for flexible geothermal operations.

2. LITERATURE REVIEW

Due to the relatively recent interest in dispatchable geothermal resources, we have found only limited studies and field implementations in the direction of flexible geothermal operations. We reviewed these implementations to develop an understanding of what options are available to achieve dispatchable geothermal operations.

Globally, researchers and engineers across different geothermal institutes and organizations have followed different approaches to achieve dispatchable geothermal operations. Recognizing that economic feasibility is essential, technical variability across methods is mainly governed by the geothermal reservoir and power plant configuration. Conventional geothermal reservoirs are generally either liquid-dominated or vapor-dominated, depending on which phase/s is mobile in the subsurface porous media. It is important to note that most global geothermal resources are liquid-dominated. Other nonconventional geothermal resources also exist, such as

enhanced geothermal systems (EGS), but they are less common and under ongoing research and development (Olasolo et al. 2016). Geothermal power plants are commonly classified into three main categories: dry steam, flash steam, and binary cycle (Augustine et al. 2019). Although they are less common, other power plant configurations also exist, e.g., multi-flash, combined-cycle, amongst others (Dipippo 2012). Optimal reservoir management and production engineering are governed by the type of the associated geothermal resource. Also, each power plant configuration is characterized with different operating requirements and power generation efficiencies. Hence, in addition to the economic viability, it is inevitable to consider both in pursuit of dispatchable operations. Based on our literature review of the studies and implementations of dispatchable geothermal energy, we classify such flexible operations into four main categories: (1) wellhead throttling, (2) steam vent-off, (3) turbine bypass, and (4) storage.

2.1 Wellhead Throttling

Starting at the upstream side of geothermal operations, one approach for dispatchability is to throttle or choke the producer wellhead valves. Hence, the total field geofluid mass flow rate from the wellsite into the power plant is reduced, and subsequently power plant generation is curtailed. Aside from adjusting the power plant operating conditions, this approach advantageously limits intervention to the wellsite and requires minimal capital investment. On the downside, it is associated with further operational expenditure, and either manual cranking of the wellhead valves or the installation of automated wellhead choke valves. Also, throttling raises wellbore integrity concerns. In diurnal flexible production, wellhead throttling causes frequent temperature and pressure cycling and stresses. This can ultimately lead to frictional sliding and material yielding at the wellbore casing, which would require costly workover operations to mitigate. Another drawback is the that excessive throttling in vapor-dominated geothermal resources increases the producer wellbore pressure. This can lead to the condensation of corrosive HCl acids, in addition to liquid water whose hydrostatic overhead could prevent further flow to surface, which would require costly workover operations (e.g., gas lift) to bring the producer well back on. Similarly, wellhead throttling in liquid-dominated resources can yield wellbore pressure and temperature conditions that promote corrosive and blocking mineral scaling within the wellbore.

Funded by the California Energy Commission (CEC), a recent study evaluated the impact of wellhead throttling in vapor- and liquid-dominated geothermal reservoirs using data from The Geysers and Casa Diablo, respectively (Rutqvist et al. 2020). The simulated models of The Geysers and Casa Diablo have reservoir temperatures of nearly 240° C and 180° C, respectively. The effect of variable geothermal production was investigated by modeling reservoir-wellbore coupled flow, wellbore geomechanics, and wellbore fluid geochemistry using T2Well (Pan and Oldenburg 2014), FLAC3D (Itasca 2002), and CHILLER (Reed 1982; Reed 1998), respectively. Upon the start of production, the vapor- and liquid-dominated systems experienced the highest thermal perturbation of 195° C and 55° C, respectively, at the top few meters of the casing string. With diurnal cycling up to 40% of mass flow rate, both systems similarly experienced the highest wellbore temperature and pressure fluctuations at wellbore segments near the wellhead. Whereas the fluctuations in the liquid-dominated system were minimal, wellbore cement temperature and pressure in the vapor-dominated system fluctuated by nearly 5° C and 2 MPa, respectively. The study concluded it is mechanically reasonable to partially throttle wellheads in low-enthalpy systems, but with a much lesser degree in high-enthalpy systems which were found to yield significant nonlinear mechanical responses in the casing with potential frictional sliding and material yielding. However, completely shutting the wellbore was found too detrimental to the wellbore integrity regardless of the system. Meanwhile, geochemical modelling showed that scaling is manageable in systems with low salinities (< 2,000 ppm TDS), where it is controlled by maintaining the wellbore pressure and temperature above the silica saturation conditions.

2.2 Steam Vent-Off

In dry steam and flash power plants, steam vent-off is achieved by diverting steam to a silenced atmospheric vent. Although it is simple, this approach is not sustainable due to the significant loss of energy and inefficiencies, especially in electricity grids with high penetration of intermittent resources and significant diurnal variability. Uncontrolled steam venting may also raise environmental and social concerns, especially in neighboring populated areas.

One of the early encounters of using steam vent-off to achieve load-following geothermal power generation dates to 1978 in the Tongonan geothermal field in the island of Leyte, the Philippines, where the 112MW Tongonan I power plant was constructed to exploit a liquid-dominated geothermal resource (Minson et al. 1985). Because it was the only large power generation plant feeding the Leyte transmission and distribution network, it had to operate in flexible mode to maintain reliability and simultaneously provide grid voltage and frequency control. To successfully achieve load-following power generation, the Tongonan I power plant was equipped with control systems to divert steam from seven control wells for vent-off and control steam turbine inlet pressure. A more recent example is the 90 MW Theistareykir geothermal power plant which started full operations in 2018 to exploit a geothermal resource in northeast Iceland (Hardarson et al. 2018). Theistareykir was built with the requirement to respond reliably to load fluctuations and maintain grid stability. Steam control valves were installed to allow for diverting and venting the separated steam into steam silencers. Meanwhile, separated water is reinjected into the reservoir.

2.3 Turbine Bypass

Bypassing steam or gas turbines is a common approach towards flexible geothermal power generation. In steam or flash power plants, the dry or separated steam is diverted to bypass the steam turbine into the condenser. In binary plants, either the geofluid is diverted away from the heat exchanger and into reinjector wells, or binary working fluid is diverted away from the gas turbine and into the condenser. In combined-cycle power plants, a combination of geofluid, steam, and binary working fluid diversion can be incorporated to achieve flexible power generation. The Geysers is a prominent example where annual levels of curtailment between 2013 and 2018 ranged between 9 to 47 GWh, representing 0.15% to 0.81% of the net generation (Dobson et al. 2020). Whereas the need for curtailment was mainly due to negative pricing and transmission line congestion across the power plant substation, Calpine, the operator of The Geysers power plants, resorted to steam turbine bypass into the condenser to achieve 100% dispatch while maintaining nearly steady-state conditions in the steam field.

An early precedent for this dispatchability approach is the Puna geothermal field run by Ormat Technologies, Inc. in Hawaii, where the operator provides dispatchable geothermal to the islanded power grid (Nordquist et al. 2013). As seen in Figure 1, the power plant

was developed with an integrated geothermal combined cycle unit, where each consists of a combined cycle and a bottoming binary cycle. The two-phase geofluid first enters the combined cycle where it is: (1) separated into steam and water, (2) steam runs a back-pressure steam turbine to generate power, (3) existing condensate from steam turbine is run into a vaporizer-preheater train to boil a binary working fluid which generates more power by spinning a gas turbine. Simultaneously, the flash-separated water is pumped into a bottoming binary cycle where it goes through a vaporizer-preheater train to boil another working fluid which spins a gas turbine and generate additional power. Ultimately, all water in the vaporizer-preheater trains is reinjected. As seen in Figure 1, pink paths show routes through which the power plant operator achieves flexible generation. Note that pink paths labeled as "1" are used to bypass binary working fluid away from gas turbines while the pink path labeled as "2" is used to bypass separated steam away from the steam turbine. Working fluid bypass is the primary means of dispatchability in the Puna geothermal power plant as it is contractually designed to provide capabilities for 2 MW ramp up/down per minute and 3 MW spinning reserves. In the event of increased grid frequency situations, steam turbine bypass is also utilized to curtail power generation more rapidly.

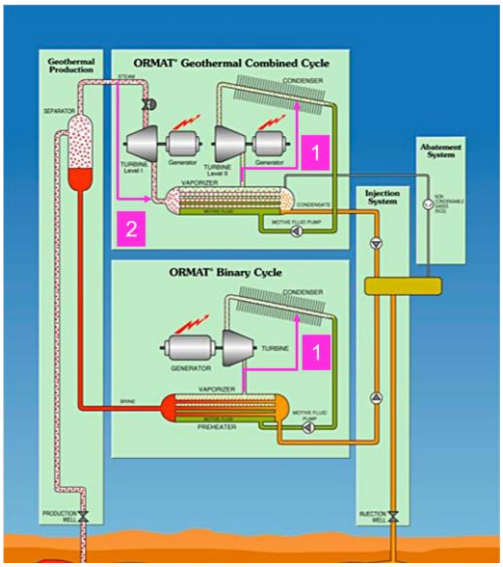

Figure 1: Ormat Technologies, Inc. design of an integrated combined cycle power plant in Puna geothermal field, Hawaii. Pink lines indicate means of achieving flexible generation, where paths are labelled "1" and "2" to represent the bypass of binary working fluid or steam, respectively (Nordquist et al. 2013).

2.4 Storage

Thermal storage could be on surface or underground. Surface energy storage can take different forms (e.g., electrochemical, mechanical, thermal, etc.), where the storage facility is charged and discharged during off- and on-peak hours, respectively. Our literature review shows only one project, called GeoSmart, that is evaluating surface storage thermal energy. GeoSmart, funded by the European program H2020, is an ongoing research and development project that aims at optimizing and demonstrating flexibility and efficiency of geothermal energy for power generation and district heating (Garabetian 2021; Petursdottir et al. 2020). One objective targeted by GeoSmart is to demonstrate retrofitting existing geothermal power plants with surface tank storage towards flexible generation. Two demonstration sites were selected: Kizildere field in Turkey (high enthalpy), and Balmatt field in Belgium (low enthalpy). Figure 2 shows the proposed design for flexible power and heat co-production at Kizildere field with two surface storage tanks for high-enthalpy steam and low-enthalpy liquid storage. As of the time of writing, the GeoSmart project is still under development (TWI 2020).

Meanwhile, efforts on underground storage, such as in-reservoir and borehole thermal storage, almost exclusively target seasonal storage with very limited studies addressing diurnal geothermal power dispatchability. A recent study proposed to store energy in the form of accumulated, pressurized geofluid in EGS reservoirs to allow for generation time-shifting through the control of production and injection rates to achieve diurnal flexibility (Ricks et al. 2022). Nevertheless, this approach also requires surface tanks to accommodate the difference between production and injection rates and enable generation time-shifting.

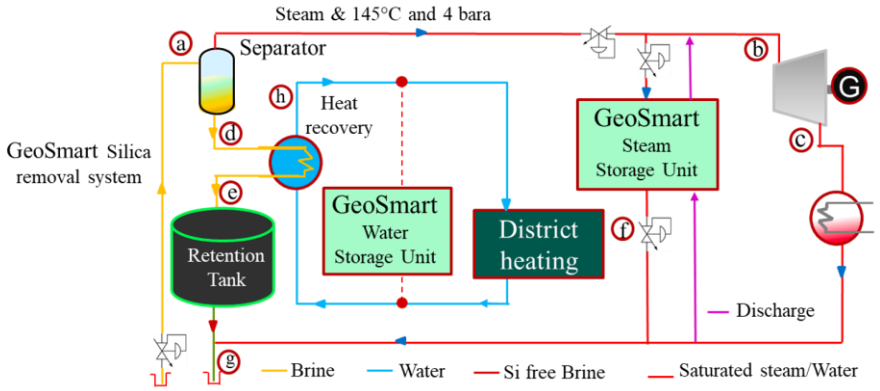

Figure 2: Surface tank storage and silica removal retrofits to the Kizildre power plants as proposed under the GeoSmart project (TWI 2020).

3. PROBLEM FORMULATION

Since the start of the 21st century, most newly built geothermal power plants in the US have been binary as they are suitable for power generation from the more common low-enthalpy resources and provide a closed system with zero emissions (Linga 2019). Therefore, we considered a binary power plant in our problem definition, although it is straightforward to modify it for flash or combined cycle power plants. As seen in Figure 3, produced geofluid flows from one or more producer wells at variable mass flow rates, passes through a heat exchanger (e.g., vaporizer and preheater train) to boil a binary working fluid, and gets reinjected at one or more injector wells with variable mass flow rates. The boiling binary working fluid spins a turbine to generate power then runs through a dry condenser before reentering the heat exchanger train. We assumed the absence of a PPA, where revenue is earned by selling the generated power to one or more electricity markets. In this paper, we consider only the real-time (RT) market as the revenue stream to evaluate economic viability, where consideration of other electricity markets is left for future work.

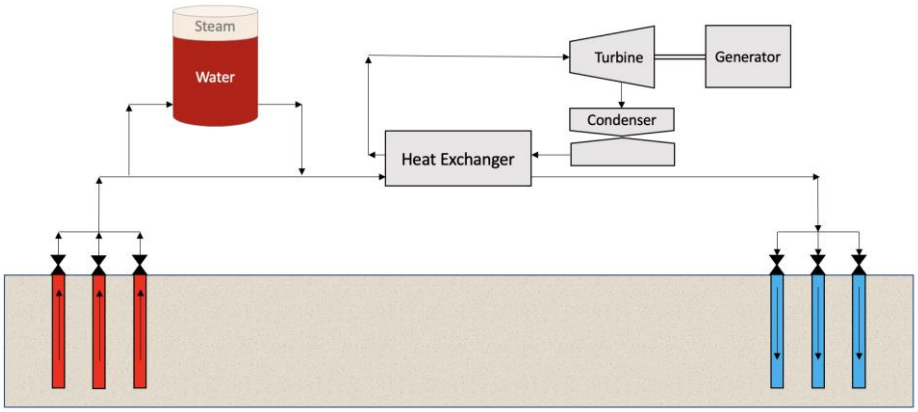

Figure 3: Simplified drawing of a binary power plant, including surface storage tank as means of flexible power generation.

We categorize the problem parameters into fixed variables, state variables, and decision/action variables. Fixed variables ($\boldsymbol{f}$) include the initial development design, i.e. subsurface geothermal resource properties or model, number of producers (N_{prd}), number of injectors (N_{inj}), wellbore configurations, nameplate power plant capacity (PPC), and capacity factor (CF). These variables remain constant throughout the dispatch scheduling process. State variables ($\boldsymbol{s}$) vary over time (t) and must be computed for each timestep Δt. They can be divided into three categories: upstream, downstream, and electricity market. Upstream state variables are associated with the reservoir and wellbore conditions, i.e. reservoir pressure (P_t^r) and temperature (T_t^r). Downstream state variables relate to the power plant output, i.e. ambient temperature (T_t^{amb}), injection water temperature (T_t^{inj}), geofluid consumption efficiency (η_t^{pp}), tank heat loss rate ($\dot{Q}_t^{HL}$) and steam quality (x_t) at thermodynamic equilibrium, and mechanical limits of ramp up/down rate (UC_t^{ramp}). State variables also involve the state of electricity market, i.e. RT market prices (p_t^{RT}). Lastly, decision/action variables ($\boldsymbol{a}$) are quantities determined by the optimizer with the objective of maximizing the economic value of the flexible geothermal power plant operations. Besides the tank height (H) and diameter (D), decision/action quantities are temporal, particularly producer well mass flow rates ($\dot{m}_t^{prd}$), injector well mass flow rates ($\dot{m}_t^{inj}$), and tank charge ($\dot{m}_t^{charge}$) and discharge ($\dot{m}_t^{discharge}$) mass flow rates.

3.1 Economics Parameters

To evaluate the profitability of flexible generation scenarios, we should also define the economic parameters. With lifetime of N_l years and inflated nominal discount rate d, the objective is to maximize the net present value (NPV) defined as the sum of discounted annual profits, seen in $NPV = \sum_{n=0}^{N_l} \frac{R_n - C_n}{(1+d)^n}$

Eq 1-6. For a given year n, annual profits are defined as the difference between the annual revenue (R_n) and annual cost (C_n). The latter is calculated as the sum of the annual short-run marginal cost ($SRMC_n$) of total annual generation (G_n), and fixed

cost of capacity ($FCOC_n$) which is constant over years. Since geothermal power does not involve carbon emission and fuel costs, $SRMC_n$ is equal to the variable operation and maintenance cost (VOM_n) minus production tax credit (PTC_n). Meanwhile, $FCOC_n$ is constant over years and equal to the sum of the levelized cost of capacity ($LCOC_n$) and fixed operation and maintenance cost (FOM_n) minus investment tax credit (ITC_n). We use the cost recovery factor (CRF) to calculate $LCOC_n$ for overnight capacity cost C_{cap} including surface storage tank cost. As seen in $LCOE = \frac{\sum_{n=0}^{N_l} \frac{C_n}{(1+d)^n}}{\sum_{n=0}^{N_l} \frac{G_n}{(1+d)^n}}$ Eq 7, we can also calculate the levelized cost of energy ($LCOE$) based on the project annual expenditure and power generation. Meanwhile, R_n is calculated as the revenue from the RT market based on generation schedule and RT spot prices, as seen in $Rn = \sum_t^{8760} \sum_i G_{\{t,i\}}^{RT} \cdot p_{\{t,i\}}^{RT}$ Eq 8, where $G_{\{t,i\}}^{RT} = G_{\{t,i\}}$ since the RT market is assumed to be the sole revenue stream in this setting.

$$NPV = \sum_{n=0}^{N_l} \frac{R_n - C_n}{(1+d)^n} \quad \text{Eq 1}$$

$$C_n = SRMC_n \cdot G_n + FCOC_n \cdot PPC \quad \text{Eq 2}$$

$$SRMC_n = VOM_n - PTC_n \quad \text{Eq 3}$$

$$FCOC_n = LCOC_n + FOM_n - ITC_n \quad \text{Eq 4}$$

$$LCOC_n = CRF \cdot C_{cap} \quad \text{Eq 5}$$

$$CRF = \frac{d \cdot (1+d)^{N_l}}{(1+d)^{N_l} - 1} \quad \text{Eq 6}$$

$$LCOE = \frac{\sum_{n=0}^{N_l} \frac{C_n}{(1+d)^n}}{\sum_{n=0}^{N_l} \frac{G_n}{(1+d)^n}} \quad \text{Eq 7}$$

$$R_n = \sum_t^{8760} \sum_i G_{\{t,i\}}^{RT} \cdot p_{\{t,i\}}^{RT} \quad \text{Eq 8}$$

3.2 Physics Parameters

This problem requires the definition of a subsurface model to simulate temperature decline, binary power plant model to simulate the geofluid consumption and reinjection fluid conditions, and a thermal storage model to simulate heat losses and thermodynamic equilibrium across the surface storage tank. Whereas we adopted conceptual models and correlations to simulate temperature decline and binary power plant efficiency, we built heat loss and thermodynamic equilibria models to simulate thermal storage.

3.2.1 Temperature Decline Conceptual Model

Because this problem setup of flexible generation does not involve wellhead throttling, then producer and injector mass flow rates $\dot{m}_t^{prd}$ and $\dot{m}_t^{inj}$, respectively, are held constant. Therefore, we can assume a simple reservoir temperature decline based on an initial reservoir temperature and fixed decline rate ρ across timesteps. Neglecting wellbore heat losses, $T_{t+1}^{prd} = (1-\rho)\, T_t^{prd}$ Eq 9 describes the producer wellhead temperature T_t^{prd} over time which is assumed to be identical across all producer wells. Whereas Figure 4 shows T_t^{prd} plotted for different decline rates ρ starting at initial reservoir temperature of $T_0^{prd} = 200° C$, we will assume a value of $\rho = 0.01$ in this paper.

$$T_{t+1}^{prd} = (1-\rho)\, T_t^{prd} \quad \text{Eq 9}$$

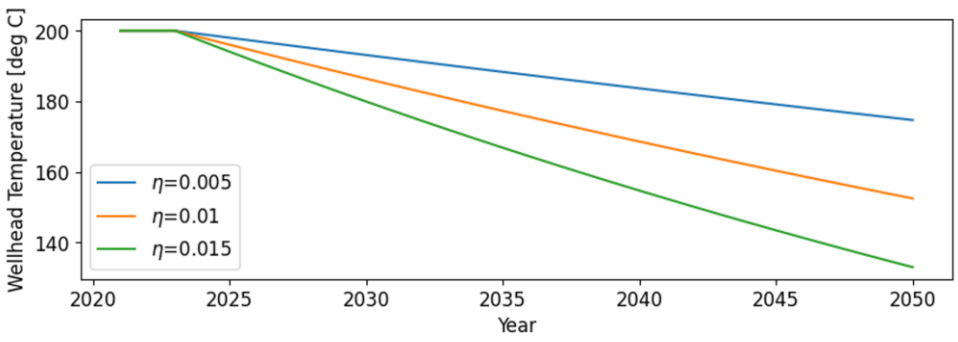

Figure 4: Simplistic percentage decline reservoir model with initial reservoir temperature of $T_0^{prd} = 200° C$ and three years of constant plateau prior to the start of decline.

3.2.1 Power Plant Correlations

We consider a subcritical Organic Rankine Cycle (ORC) power plant modeled using correlations originally developed for GEOPHIRES, a geothermal project economics module produced by NREL scientists (Beckers and McCabe 2019). This correlation predicts the power plant geofluid consumption η_t^{pp} and reinjection water temperature T_t^{inj} for different combinations of wellhead

temperature T_t^{prd} and ambient temperature T_t^{amb}. Figure 5 shows the power plant output, geofluid consumption, and reinjection water temperature T_t^{inj} for selected ranges of wellhead temperature T_t^{prd} and ambient temperature T_t^{amb}.

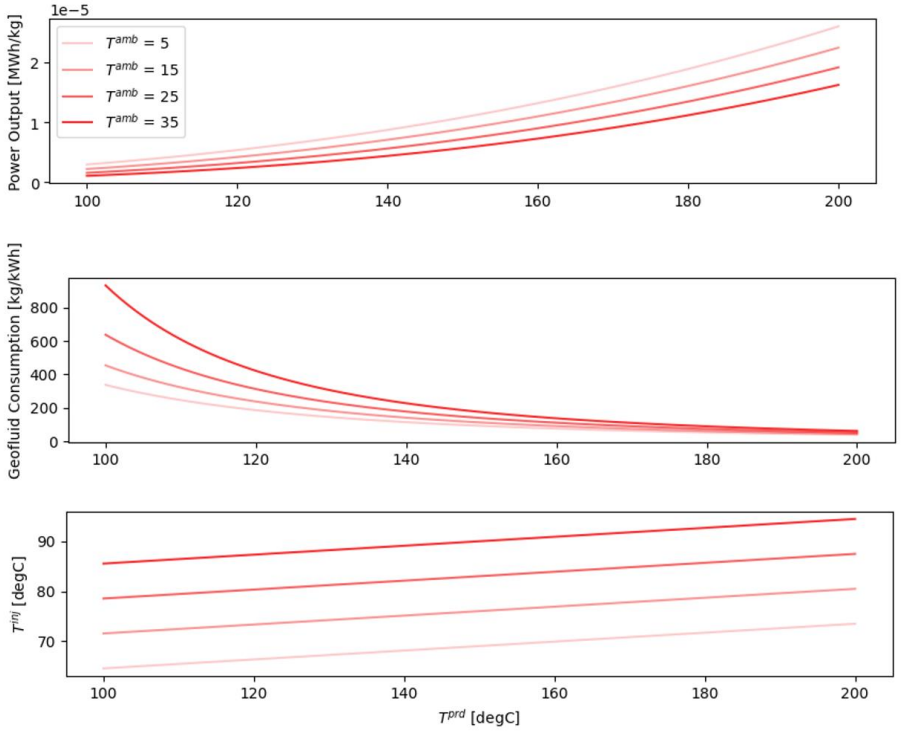

Figure 5: Subcritical ORC power plant correlations for power output, geofluid consumption, and reinjection (Beckers and McCabe 2019).

3.2.1 Thermal Storage Model

Tank heat losses at each timestep Δt are computed based on heat transfer principles of conduction, convection, and radiation (Orsini et al. 2021; Lienhard and John 2005; Bergman et al. 2011). As seen in Figure 6, we consider an insulated steel tank of height H, diameter D, top/bottom surface area A^{roof}, sides surface area A^{sides}, steel inner and outer radii $r^{\{in,st\}}$ and $r^{\{out,st\}}$, insulation inner and outer radii $r^{\{in,ins\}}$ and $r^{\{out,ins\}}$, steel wall thickness L^{st}, and insulation wall thickness L^{ins}. The tank is assumed to have steady material temperature for small infinitesimally timestep Δt. At each Δt, we perform two steps: (1) heat transfer, and (2) thermodynamic equilibrium calculations.

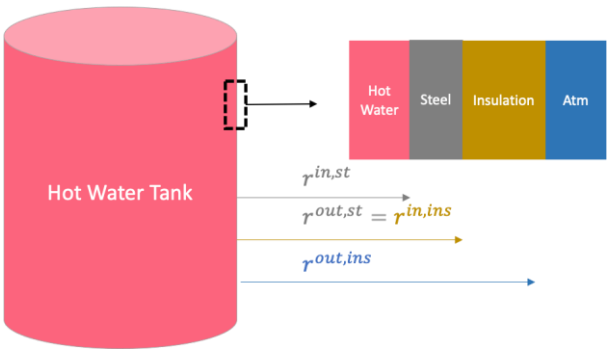

Figure 6: Insulated steel thermal storage tank, where heat losses are considered across the side and top/bottom walls.

We first addressed the heat loss calculations using heat transfer principles. As seen in $\dot{Q}^{cond,st} = \dot{Q}^{cond,ins} = \dot{Q}^{conv} + \dot{Q}^{rad}$ Eq 10-16, the conductive heat loss rate across the steel wall $\dot{Q}^{cond,st}$ is then equal to the conductive heat loss rate across the insulation wall $\dot{Q}^{cond,ins}$, and also equal to the total convective $\dot{Q}^{conv}$ and radiative $\dot{Q}^{rad}$ heat loss rates to the atmosphere (Note that we omit subscript t for convenience). Conductive heat losses are driven by the thermal conductivity coefficients k^{st} and k^{ins}, and include those at the sides $\dot{Q}^{cond,i,sides}$, top $\dot{Q}^{cond,i,top}$, and bottom $\dot{Q}^{cond,i,btm}$ $\forall\ i \in \{st, ins\}$. Also, convective $\dot{Q}^{conv}$ and radiative $\dot{Q}^{rad}$ heat loss rates are calculated as functions of T^{amb} and A^{sides} using the convective heat transfer coefficient u and the Stefan-Boltzmann constant σ, respectively. This is a system of two equations and two variables which we solve analytically to find $T^{st}(r^{out,st})$, $T^{ins}(r^{out,ins})$, and $\dot{Q}^{cond,st}$. Using the system heat loss rate, i.e. $\dot{Q}^{cond,st}$, we can finally calculate the tank temperature drop ΔT^{tank} for a timestep Δt using the water and steam isobaric specific heat capacities and mass inside the tank, i.e. $c^w, c^s, m^{tank,w}$ and $m^{tank,s}$, respectively.

$$\dot{Q}^{cond,st} = \dot{Q}^{cond,ins} = \dot{Q}^{conv} + \dot{Q}^{rad} \quad \text{Eq 10}$$

$$\dot{Q}^{cond,i} = \dot{Q}^{cond,i,sides} + \dot{Q}^{cond,i,top} + \dot{Q}^{cond,i,btm} \quad \text{Eq 11}$$

$$\dot{Q}^{cond,i,sides} = \frac{2\pi H k^i [T^i(r^{in,i}) - T^i(r^{out,i})]}{\ln \frac{r^{out,i}}{r^{in,i}}} \quad \forall\ i \in \{st, ins\} \quad \text{Eq 12}$$

$$\dot{Q}^{cond,i,j} = \frac{A^{roof} k^i [T^i(r^{in,i}) - T^i(r^{out,i})]}{L^i} \quad \forall\ i \in \{st, ins\}\ \ and\ \ \forall\ j \in \{top, btm\} \quad \text{Eq 13}$$

$$\dot{Q}^{conv} = A^{sides} u\ [T^{ins}(r^{out,ins}) - T^{amb}] \quad \text{Eq 14}$$

$$\dot{Q}^{rad} = A^{sides} \sigma\ [\ T^{ins}(r^{out,ins})^4\ - (T^{amb})^4] \quad \text{Eq 15}$$

$$\Delta T^{tank} = \frac{\dot{Q}^{cond,st} \cdot \Delta t}{c^w\ m^{tank,w} + c^s\ m^{tank,s}} \quad \text{Eq 16}$$

In modelling heat losses, we require the knowledge of water and steam mass inside the tank at each timestep. Hence, we also need to run flash calculations to establish thermodynamic equilibrium, and account for energy and mass balance with respect to the tank. As seen in Eq 17, we use control volume around the tank over each timestep Δt and account for the enthalpy flow in/out of the tank, enthalpy accumulation, and heat losses. As seen in Eq 18, we similarly formulate the mass balance around the storage tank. Given the tank volume V^{tank}, we must also establish thermodynamic water-steam equilibrium after each timestep Δt by accounting for the two-phase specific volume v and steam quality x, seen in Eq 19-20. Note that enthalpy h_t and specific volume v_t are implicitly estimated using steam tables (Holmgren 2006) as functions of T_t^{tank} which also changes over time. Finally, we solve for $m_{t+\Delta t}^w$, $m_{t+\Delta t}^s$, and $T_{t+\Delta t}^{tank}$. This is solved iteratively by minimizing the sum of squared residuals of the system equations (Virtanen et al. 2020; Garbow 1984).

$$(m_{t+\Delta t}^w\ h_{t+\Delta t}^w + m_{t+\Delta t}^s\ h_{t+\Delta t}^s) - (m_t^w\ h_t^w + m_t^s\ h_t^s) = \left(\dot{m}_t^{charge} h_t^{charge} - \dot{m}_t^{discharge} h_t^{discharge} - \dot{Q}_t^{cond,st}\right) \Delta t \quad \text{Eq 17}$$

$$(m_{t+\Delta t}^w + m_{t+\Delta t}^s) - (m_t^w + m_t^s) = \left(\dot{m}_t^{charge} - \dot{m}_t^{discharge}\right) \Delta t \quad \text{Eq 18}$$

$$v_{t+\Delta t}^{tank} = \frac{V^{tank}}{m_{t+\Delta t}^w + m_{t+\Delta t}^s} \quad \text{Eq 19}$$

$$x_{t+\Delta t} = \frac{m_{t+\Delta t}^s}{m_{t+\Delta t}^w + m_{t+\Delta t}^s} = \frac{v_{t+\Delta t}^{tank} - v_{t+\Delta t}^w}{v_{t+\Delta t}^s + v_{t+\Delta t}^w} \quad \text{Eq 20}$$

3. CASE STUDY

Using the database of the California Independent System Operator (CAISO), we retrieved the 2021 locational marginal price (LMP) records for the RT market with five-minute frequency across all three California trading hubs (THs): TH_NP15, TH_ZP26, and TH_SP15. The highest LMP record across trading hubs was at nearly 1,200 $/MWh with considerable variability. Figure 7 shows annual LMP distribution across trading hubs for records less than 200 $/MWh, where the average annual price across zones is 43 $/MWh. The distribution is bimodal, where negative prices are common because of the high penetration of solar resources into the California grid. The frequency of negative prices across TH_NP15, TH_ZP26, and TH_SP15 is 2.4%, 4.7%, and 4.1%. Figure 8 shows the hourly distribution of negative pricing occurrence per quarter. We observe that negative pricing hours almost exclusively occur around noon. Also, the highest occurrence rates of negative pricing hours are during the Spring season, when solar and hydroelectric generators are most prolific. Meanwhile, the least frequency of negative prices is observed during the summer season due to the decrease in power supply (i.e. warmer ambient temperatures lead to lower power plant efficiencies) and increase in demand due to the use of air conditioning during the daytime. We also retrieved the 2021 weather conditions at the same locations. Figure 9 shows LMP, ambient temperature and wind speed across three random days in TH_ZP26 which clearly demonstrates the infamous "duck curve" pattern.

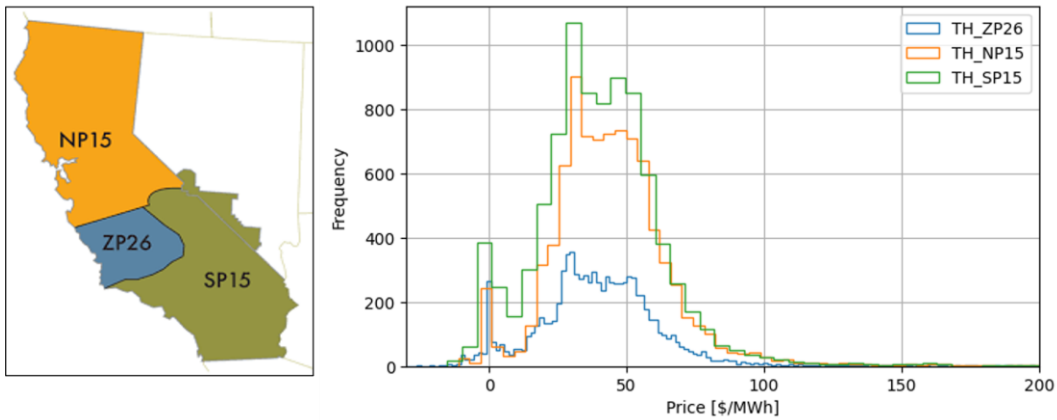

Figure 7: Distribution of 2021 LMP records of the CAISO RT market across TH_NP15, TH_ZP26, and TH_SP15.

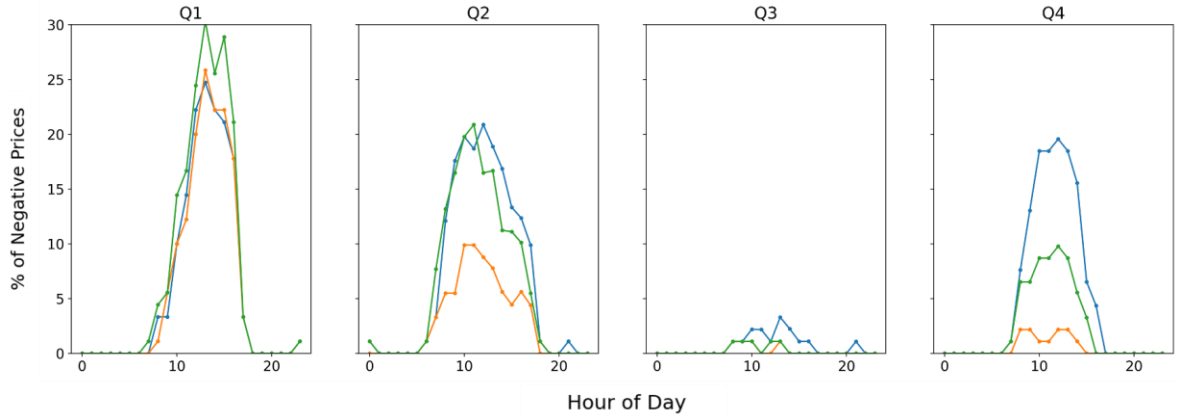

Figure 8: Hourly distribution of 2021 CAISO RT market negative price occurrence across TH_NP15, TH_ZP26, and TH_SP15.

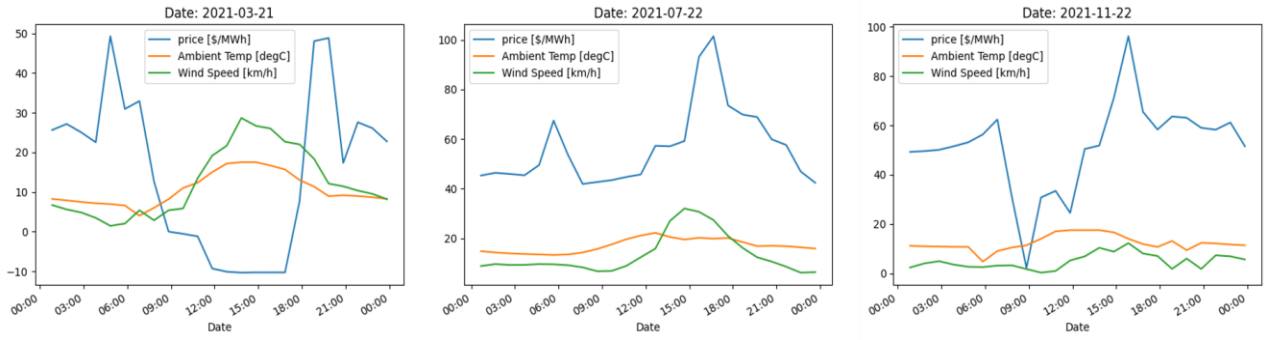

Figure 9: LMP, ambient temperature, and wind speed across three random days of 2021 in TH_ZP26.

We considered a 200° C, liquid-dominated geothermal resource developed with five producers and five injectors with steady-state production $\dot{m}_t^{prd} = 150\ kg/s$ and capacity factor $CF = 90\%$. With inflated nominal discount rate $d = 0.11$, we considered levelized annual capacity operational costs of 15 $\$million/year$ and 4 $\$million/year$, respectively. We considered the 2021 LMP records of TH_ZP26 as it involves the highest frequencies of negative pricing. We assumed LMP records repeat annually and follow the same patterns throughout the project lifetime of $N_l = 30\ years$. With an 80-MW subcritical ORC power plant and cost estimates provided by Beckers and McCabe (2019), we found project $LCOE$ of 43 $\$/MWh$. If the project operator were offered a PPA, they would have to secure a minimum of 43 $\$/MWh$ PPA price to reach the break-even point of zero NPV. With a typical PPA price of nearly 70 $\$/MWh$, this geothermal operator would make 116 $\$million$ in NPV. However, we are interested in scenarios where a geothermal operator could not secure a PPA, or where a PPA involves a clause awarding flexible generation to cope with the CAISO system which is nowadays highly penetrated by intermittent renewables.

We first established the baseline case (Scenario #1), where the geothermal power plant operates in baseload mode and sells all generation at the RT market clearing price. The power plant bids to the RT market are assumed to be always accepted by CAISO. With nominal discount rate $d = 0.11$, this operating strategy/policy yields a losing project with $NPV = 8.23\ \$million$. Similarly, we considered a slightly improved strategy (Scenario #2) where the operator chooses to vent out steam during negative pricing hours

while assuming the operator does not incur any additional operational costs. By design, Scenario #2 is strictly better than Scenario #1, but still results in a losing project with $NPV = -7.54\ \$million$.

Figure 10 compares baseload generation and revenues based on $70\ \$/MWh$ PPA versus the Scenario #2 flexible generation. We first note that the power plant output is lower during the summer season due to the warmer ambient temperatures. Additionally, the power plant output decreases over years because of the depleting geothermal subsurface resource, seen in Figure 4. While the PPA hourly revenues are solely driven by the power plant output because the PPA price is fixed, the Scenario #2 hourly revenues are mainly driven by the RT market LMPs. Consequently, the PPA hourly revenues experience a relative decrease while the Scenario #2 hourly revenues relative increase during the summer season.

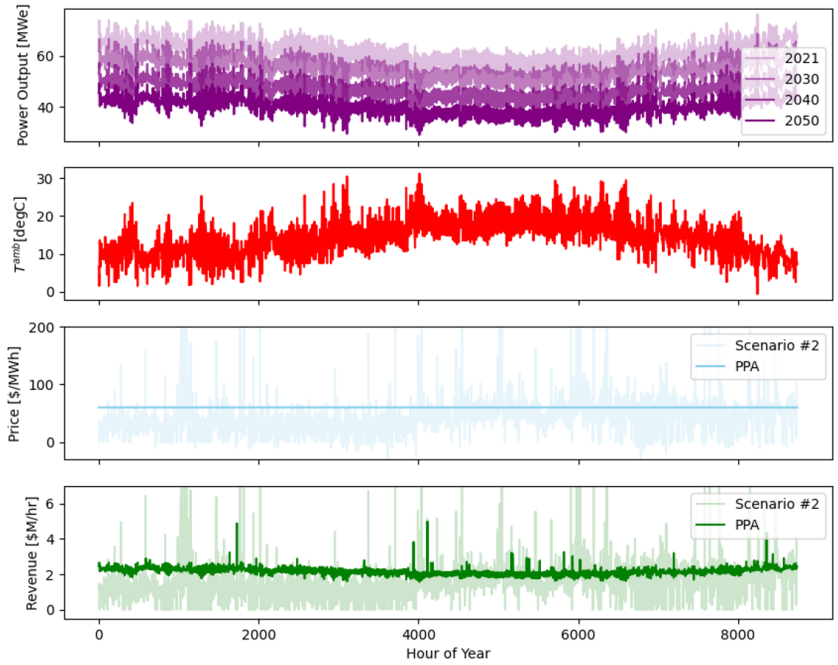

Figure 10: Plot of power plant output, T^{amb}, RT market LMP, and hourly revenue for geothermal power generation and revenues under PPA versus Scenario #2 flexible generation with no PPA.

Next, we evaluated the profitability of flexible geothermal generation using a surface thermal storage tank. Note that we only provide an example strategy without performing any form of optimization. In this scenario (Scenario #3), flexible generation is enabled using a surface thermal storage tank with $H = 13\ m$, $D = 34\ m$, $L^{st} = 0.08\ m$, $L^{ins} = 0.05\ m$, $k^{st} = 45\ W/(mK)$, $k^{ins} = 0.17\ W/(mK)$, and $u = 13\ W/(m^2K)$. The tank is treated as a commercial pressure vessel with cost that is linearly correlated to its volume based on estimates by Orsini et al. (2021). The described tank in this demonstration can hold $11{,}830\ m^3$ which costs nearly $17\ \$million$. This is then levelized using CRF with $d = 0.11$ and $N_l = 30\ years$, translating to an annual levelized tank capital cost of nearly $1.98\ \$million/year$.

In Scenario #3, we considered a practical dispatch strategy like the "Model_4" strategy proposed by Millstein et al. (2021), in which the tank is charged daily during the four hours with the lowest prices and discharged during the 16 hours of the highest prices. Nevertheless, the total power output is constrained by the maximum available nameplate capacity. The NPV of operating in this mode is $0.87\ \$million$, which is a total of $8.41\ \$million$ over that of Scenario #2; hence, the project is profitable if operated under flexible generation in the absence of a PPA. Nevertheless, it is still not profitable enough to attract investment. Figure 11 shows the Scenario #3 strategy in action for five randomly chosen days during the Spring season. We notice that storage tank is charged during lower price hours (mostly around noon) and discharged during the higher price hours. We also note that the water volume in the tank $V^{tank,w}$ is limited to the 95% of the tank size as a maximum and $250\ m^3$ as a minimum, which is important to respect tank construction limitations and limit the occurrence of vacuum inside the tank.

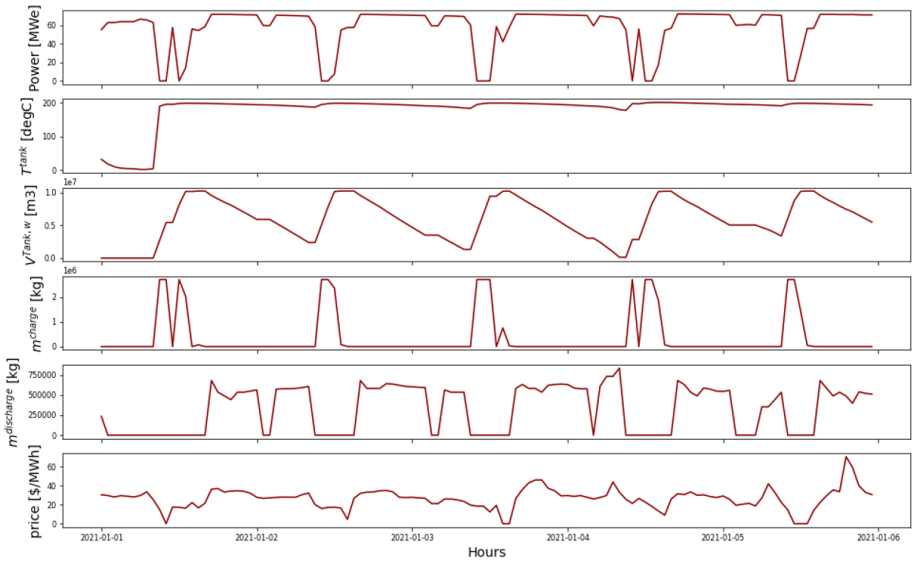

Figure 11: Dispatch strategy of Scenario #3 in action for five randomly chosen days during the Spring season.

3. CONCLUSIONS

In this work, we investigated the techno-economic viability of installing surface thermal storage tanks to enable flexible geothermal generation. We examined a 200° C, liquid-dominated geothermal resource developed with five producers and five injectors alongside an 80-MW subcritical ORC power plant. A 11,830 m^3 surface thermal storage tank is incorporated into the system. We backtested the techno-economic performance of such system in 2021 real-time electricity market prices using a strategy in which the tank is charged daily during the four hours with the lowest prices and discharged during the 16 hours of the highest prices. Results indicate that flexible generation results in NPV increase of 8.41 $\$million$ compared to the baseline scenario of baseload power generation during positively priced time intervals. Whereas this is still short of the profits typically achieved under PPAs, it demonstrates the potential of operating geothermal facilities to supply grids that are islanded and/or highly penetrated with intermittent resources.

REFERENCES

C. Augustine, J. Ho, and N. Blair. Geovision analysis supporting task force report: Electric sector potential to penetration. Technical report, National Renewable Energy Lab (NREL), Golden, CO, 2019.

K. Beckers and K. McCabe. GEOPHIRES v2. 0: updated geothermal techno-economic simulation tool. Geothermal Energy, 7(1):1–28, 2019.

T. Bergman, Theodore Bergman, Frank Incropera, et al. Fundamentals of heat and mass transfer. John Wiley & Sons, 2011.

R. DiPippo. Geothermal power plants: principles, applications, case studies and environmental impact. Butterworth-Heinemann, 2012.

P. Dobson, D. Dwivedi, D. Millstein, et al. Analysis of curtailment at the geysers geothermal field, California. Geothermics, 87:101871, 2020.

T. Garabetian. Flexibility services and capacity availability: Towards a business model and regulatory framework for geothermal orc plant market uptake. In Proceedings of the 6th International Seminar on ORC Power Systems, 2021.

B. Garbow. Minpack-1, subroutine library for nonlinear equation system. 1984.

F. Hardarson, B. Heimisson, S. Geirsson, et al. Theistareykir geothermal power plant, challenges in a weak electrical grid. GRC Transactions, 42, 2018.

M. Holmgren. X steam for MATLAB. www. x-eng. com, accessed October, 21:2006, 2006.

H. Itasca. FLAC3D (fast lagrangian analysis of continua in 3 dimensions). Computer Program, 2002.

I. Lienhard and H. John. A heat transfer textbook. phlogiston press, 2005.

V. Linga. Most us utility-scale geothermal power plants built since 2000 are binary-cycle plants. 2019.

D. Millstein, P. Dobson, and S. Jeong. The potential to improve the value of us geothermal electricity generation through flexible operations. Journal of Energy Resources Technology, 143(1), 2021.

A. Minson, J. Kivell and T. Fry. Tongonan I geothermal power development, philippines. Geothermics, 14(2-3):353–370, 1985.

J. Nordquist, T. Buckanan and M. Kaleikini. Automatic generation control and ancillary services. GRC Transactions, Las Vegas, NV, Sept, 2013.

P. Olasolo, M. Juarez, M. Morales, et al. Enhanced geothermal systems (EGS): A review. Renewable and Sustainable Energy Reviews, 56:133–144, 2016.

R. Orsini, P. Brodrick, A. Brandt, et al. Computational optimization of solar thermal generation with energy storage. Sustainable Energy Technologies and Assessments, 47:101342, 2021.

L. Pan and C. Oldenburg. T2well—an integrated wellbore–reservoir simulator. Computers & Geosciences, 65:46–55, 2014

A. Petursdottir, A. Massey, E. Desjardins, et al. Assessing geothermal projects using envision, GRC Transactions, Davis, CA, 2020.

M. Reed. Calculation of multicomponent chemical equilibria and reaction processes in systems involving minerals, gases and an aqueous phase. Geochimica et Cosmochimica Acta, 46(4):513–528, 1982.

M. Reed. Calculation of simultaneous chemical equilibria in aqueous-mineral-gas systems and its application to modeling hydrothermal processes. 1998.

W. Ricks, J. Norbeck, and J. Jenkins. The value of in-reservoir energy storage for flexible dispatch of geothermal power. Applied Energy, 313:118807, 2022.

J. Robins, A. Kolker, F. Flores-Espino, et al. 2021 US geothermal power production and district heating market report. Technical report, National Renewable Energy Lab (NREL), Golden, CO, 2021.

J. Rutqvist, L. Pan, N. Spycher, et al. Coupled processes analysis of flexible geothermal production from steam-and liquid-dominated systems: impacts on wells. In Proceedings, 45th Workshop on Geothermal Reservoir Engineering, Stanford University, Stanford. CA, SGP-TR-216, page 17, 2020.

TWI. Geosmart: Towards flexible and efficient geothermal systems, 2020.

P. Virtanen, R. Gommers, T. Oliphant, et al. Scipy 1.0: fundamental algorithms for scientific computing in python. Nature methods, 17(3):261–272, 2020.